Results in Physics 48 (2023) 106418

Contents lists available at ScienceDirect

Results in Physics

journal homepage: www.elsevier.com/locate/rinp

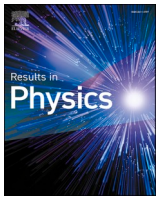

Morphological growth criterion for faceted to non-faceted transition in pure materials

Yaw Delali Bensah

Department of Materials Science and Engineering, School of Engineering Sciences, University of Ghana, PMB, Accra, Ghana

ARTICLE INFO

Keywords:
Maximum entropy generation rate density
Solidification
Faceted
Non-faceted
Morphological transition

ABSTRACT

A criterion to explain the morphological growth transition from faceted to non-faceted (*f-nf*) morphology in the case of directional solidification is presented for pure materials. The criterion is based on the number of atomic layers at the solid–liquid interface and allows a foreknowledge of the solidification growth velocity at which *f-nf* transition becomes significant. The basis for the transition criterion hinges on the Cahn theory of interface structure and the theory of liquid–solid transition by the maximum entropy production rate (MEPR) principle. The criterion is tested with a number of pure materials and compared with experimental measurements for salol. The criterion fits quite well with available experimental data.

Introduction

Over the years, the formation of directionally solidified irregularly grown faceted to non-faceted (*f-nf*) eutectics has gain much attention, especially for intermetallic compounds (IMCs) such as Al-Si, Al-Mn, Al-Sc and Fe-C binary alloys [1,2]. This has been the case as a result of its wide use in industry coupled with its greater practical importance [3]. The eutectic growth theory by Jackson and Hunt, the Sato-Sayama-Ohira model [4] and that of Kurz and Fisher [3] has deepened our understanding over the initial problem of irregularity, the isothermal nature and the mechanism involved in the growth of these eutectics. The transition model for faceted to non-faceted in IMCs indicates a kinetic interface roughening transition and a gradual change in mechanism from lateral growth governed by anisotropic attachment kinetics to continuous growth governed by diffusion and curvature [5]. It is also well known that, the addition of some alloying elements or the presence of impurity elements can cause a transition from faceted form to a non-faceted form [6-8]. In the case of pure materials, the absence of alloying elements and possible absence of impurity elements points to a reason to search for other possible explanation to the origin of the faceted to non-faceted transformation. That is, the explanation for the transformation for faceted to non-faceted morphology for IMCs may be not applicable to pure materials. However, beyond morphological instability of a plane front interface, the formation of a faceted morphology and the corresponding transformation to a non-faceted morphology for both IMCs and pure material has been bereft of a transition criterion. A knowledge of a transition criterion would be important in controlling the microstructural evolution of materials associated with both faceted and non-faceted morphologies.

The main object of this paper is to provide a criterion than accounts for the transition from faceted cellular to non-faceted cellular (*f-nf*) morphological growth during liquid–solid transformation restrictive to directional solidification of the Bridgman type for pure materials. This criterion considers that, the adjoining surface between the transforming liquid to solid is a diffuse interface and with a definite size [9,10] which can be quantified by employing tools from the principle of maximum entropy production rate [11,12].

The form of the microstructure developed during morphological evolution from a crystal-melt interface during crystal growth/solidification is one of the most important features required for obtaining high-quality materials. These materials (or crystals) which are commercially used as semiconductors and metallic alloys are grown from melts by directional solidification techniques [9,13,14]. During directional solidification of molten materials, the initial plane front interface becomes unstable at increased solidification growth velocity which then breaks down (morphological instability) to give a cellular-wavy microstructure in the solidified phase under a fixed temperature gradient. The cellular-wavy microstructure formed is of two major types; cellular-faceted and cellular-non-faceted morphology. These two types emanate from the interface which is an intersection between a fully liquid zone and a fully solid zone under controlled conditions [11,15-17]. In a two-dimensional view, the faceted morphology appears to have jagged edges whereas the non-faceted morphology has smooth rounded edges, i.e., the faceted morphology is of a zig-zag shape, whereas the non-faceted morphology is of a wavy test-tube like cellular shape. The evolution of these two

E-mail address: ydbensah@ug.edu.gh.

https://doi.org/10.1016/j.rinp.2023.106418
Received 6 January 2023; Received in revised form 4 March 2023; Accepted 29 March 2023
Available online 1 April 2023

List of symbols

General symbols

A_W (Kg/mole) atomic weight
d (m) interplanar spacing
g_m (dimensionless) Cahn diffuseness parameter
G_L (K m^{-1}) temperature gradient in the liquid
Δh_{sl} (J m^{-3}) volumetric heat of fusion
Δh_m (J mol^{-1}) heat of fusion
M_d (dimensionless) constant
T_m (K) melting temperature
V (ms^{-1}) solidification growth velocity

Greek symbols

$\dot{\varphi}_{max}$($Jm^{-3}K^{-1}s^{-1}$) maximum entropy generation rate density
$\Delta\rho_k$ (kg m^{-3}) overall density shrinkage
$\Delta\rho$ (kg m^{-3}) density change from liquid to solid
ρ_s (kg m^{-3}) density of the fully solid state
ρ_l (kg m^{-3}) density of the fully liquid sate
ζ (m) thickness of the solid–liquid interface (SLI)
η_G (dimensionless) Cahn driving force diffuseness
α_J (dimensionless) Jackson roughness factor

Acronyms

MEPR maximum entropy rate density
SLI solid–liquid interface
f faceted
nf non-faceted

morphological forms and the associated conditions haves been studied experimentally and theoretically over the years [9,13,14]. However, there is a morphological transition variant that involves a faceted cellular to non-faceted cellular (*f-nf*) transformation which has received little research attention despite its technological and theoretical importance. That is, materials that produces faceted cellular morphology at instability have the ability to transform into a non-faceted cellular morphology with an increase in solidification growth velocity and with the establishment of other relevant conditions. In spite of the many experimental evidence supporting faceted cellular to non-faceted cellular transition as summarized in Table 1, there is not much theoretical foundation underpinning this important phenomenon in pure materials.

Solid-liquid interface (SLI) diffuseness and faceted to non-faceted transition

The interface between two phases has been described in different forms by many researchers over the years. Earlier works by Young [18], Laplace [19] and Gauss [20] have treated that, the interface between two different phases is separated by a thickness of zero [21]. Thus, the physical properties such as density and concentration may change discontinuously across the interface. From the phenomenological theories of crystal growth by Wilson [22], Frenkel [23], Becker and Doring [24], and Burton, Cabrera and Frank [25], the discontinuity in properties across an interface and the zero size of the interface has been named in many literature sources a sharp phase boundary or a sharp interface.

On the other hand, the interface is also described by Rayleigh [26] and Van der Waals [27] to have non-zero thickness. Over the years, a non-zero interface has been used to described an adjoining solid–liquid interface (SLI) of definite size as diffuse, comprising of a rigorous mixture of the two different phases. Analysis by Landau [28] and Van der Waals [27] had shown that, the SLI is associated with a thermodynamic potential and it is expected to exhibit diffuseness. For the SLI during crystal growth, Cahn [10] showed that, either a sharp or diffuse interface is possible depending on the material type and growth conditions. The solid–liquid interface (SLI) was further categorized by Cahn as (*i*) atomistically smooth, which grows by lateral motion mechanism and as (*ii*) atomistically rough, which grows by continuous surface advancement without needing steps [9,10], and where transition at different velocities was feasible. On a macroscopic level, the atomistically smooth interfaces are expected to display macroscopic faceted microstructure as they rely on growth defects for propagation, such as dislocations and ledges. Similarly, the atomistically rough interfaces are expected to support continuous growth mechanisms and display macroscopically smooth curved (non-faceted) microstructure.

Prior to Cahn's model of the interface diffuseness, Jackson [29] evaluated the interaction of a liquid phase with the solid phase, and its consequences for surface roughness. Jackson's approach employed a statistical mechanical model, describing how the solidification of pure materials depend on the roughness at the atomic scale for the SLI. He gave roughness criterion as:

Table 1
Summarized experimental evidence for faceted to non-faceted transition reported for some materials by different solidification techniques.

Material	α_J	*f-nf*				Remarks
		$V_{f\text{-}nf}$ (μm)	$\Delta T_{f\text{-}nf}$ (K)	G_L (K/m)	T_R (K)	
Al_2O_3-1 *wt%* MgO [37]	5.58	6660	–	–	–	Solidified is by laser and also show *nf-f* at 8500 μm and *f-nf* at 56550 μm.
Cyclohexanol [38]	0.69	–	283		–	Cyclohexanol forms facets at small undercooling up to 283 K. Beyond 283 K a *nf-f* transition is observed.
Salol [32]	7.08	60.2	–	1100	–	Melt grown directionally solidified.
Salol [39]	7.08	–	298–302	–	286–280	The materials were melt-grown and the microstructures obtained were spherulitic. The transition could also be reversed from *nf-f* with a change in the undercooling.
O-terphenyl [39]	6.28	–	35–30	–	293–298	
Thymol [39]	8.17	–		–	263–258	
P_4 [40]	0.99	120000–450000	274–280	–	–	The material is melt-grown in isenthalpic and non uni-directional. P_4 is faceted at 274 K which becomes nonfaceted somewhere between 274 and 280 K.
Al_6CuLi_3 [41]	6.7	27	–	10,000	–	Directionally solidified.
Ge [42]	3.67	–	273–275	–	–	The non-facet and facet morphologies were in the (1 0 0) and (1 1 1) planes respectively. Material grown by the Czochralski method.
NH_4Cl [43]	2.09	–	–	–	638	Material is grown in a vapour phase in a sealed capsule at a vapour pressure of 3 atm.
C_2Cl_6 [43]	2.2	–	–	–	373	Material is grown in a vapour phase in a sealed capsule at a vapour pressure of 40 Torr.
Zn-5 *wt%* In [44]	1.26	–	–	–	523	The alloy is melt grown.
Zn-Bi-In [45]	1.26	–	–	–	–	Transition occurs at lower ratio of surface to grain boundary energy.

$$\alpha_J = \frac{\Delta h_m}{R_g T_m} \quad (1)$$

where α_J (dimensionless) is commonly called the Jackson roughness factor, Δh_m (J mol^{-1}) is the heat of fusion, Tm (K) is the melting temperature of the material and R_g ($Jmol^{-1}K^{-1}$) is the gas constant. Jackson showed that, materials with α_J greater than 2 will grow into a faceted (*f*) morphology whiles materials with α_J less than 2 will grow into a non-faceted (*nf*) morphology. The Jackson criterion has seen an appreciable success and strong correlation with experimental results for the solidification of pure materials. In spite of the successes, Jackson criterion is so simplistic and it is not without drawbacks. The first limitation of the Jackson criterion is common in materials in which α_J is with in range, $2 \leq \alpha_J \leq 3$; such materials may behave as either faceted or non-faceted depending on the crystallographic orientation. This observation has been seen in bismuth, silicon, germanium, salol, benzyl and water [30-32]. The second limitation is that, it does not take into account the effect of temperature gradient/cooling rate and changes in the solidification growth velocity, V (ms^{-1}), which is the most critical parameter during directional solidification. The third is that, it is only qualitative and gives no knowledge of the size of the interface and the number of lattice spacings (number of atomic layers) possibly present within the SLI. And lastly, it does not account for the transition from a faceted to non-faceted (*f-nf*) morphological change. On the other hand, Jackson [33] gave a quantitative definition of interface diffuseness as, $1/\alpha_J$ which generated a heated debate with Cahn. However, the issue of the use of diffuseness and roughness has never been settled or clarified, and it has been used interchangeably in the literature since then, except recently by Sekhar and Bensah who have attempted to bring a distinction between the use of the terms [11,12,16,17,34].

The formation of faceted and non-faceted morphologies can be predicted by the Jackson roughness factor, α_J (dimensionless) for pure materials [29,33,35,36] as shown by equation (1), all beginning from the plane front.

The transition of a faceted to non-faceted morphology, which is a special variant in liquid to solid phase transformation is usually observed when there is an increased in solidification growth velocity specifically under controlled conditions such as the case of directional solidification. The Table 1 gives a summary of experimental evidences for faceted to non-faceted transformation for different materials at different growth conditions though the data does not report on any criterion necessary for the transition to occur.

The Cahn theory quantitatively describes that, when the Cahn diffuseness parameter, g_m (dimensionless) is 1, then atomistically smooth interface is formed and when it is less than 1, then atomistically rough interface is formed. Cahn further showed through thermodynamic deductions that, there is a possibility of transition from faceted to non-faceted morphology, but the transition equations were difficult to use due to some inaccessible parameters. Another limitation of the Cahn's theory is that, it does not address the criterion and thermodynamic condition required for *f-nf* transition to occur either through the Cahn diffuseness parameter or the Cahn driving force diffuseness (η_G) parameter which expresses the number of atomic layers at the solid–liquid interface. The available experimental data shown in Table 1 supports Cahn's view of faceted to non-faceted transition and the dependence on the solidification growth velocity despite that, is it bereft of a transition criterion.

Model

Let us consider a control volume approach of a solidification system at steady state conditions where a fully rigorous liquid (molten state) enters the control volume at a temperature T_{li} and leaves at a temperature T_{si} into a fully rigorous solid state (crystalline state) as schematically shown in Fig. 1. The control volume bounded by the temperatures T_{li} and T_{si} which is of thickness ζ (m) and is considered as the interface (that is, the solid–liquid interface, SLI) between the fully liquid zone and the fully solid zone. Under this consideration, the solid–liquid interface is considered diffuse, where the interface is a mixture of the fully rigorous liquid particles and fully rigorous solid particles as treated by Cahn [15], Sekhar [16] and other phase field model applications [46-52]. Recent studies on pure unary material systems [11,12] showed that, an entropy balance performed across the SLI as shown in Fig. 1 at steady state conditions result in the relation given as [11,34]:

$$\dot{\varphi}_{max} = \dot{s}_E \quad (2)$$

where $\dot{\varphi}_{max}$ ($Jm^{-3}K^{-1}s^{-1}$) is the maximum entropy production rate density associated with SLI during solidification and $\dot{s}_E$ ($Jm^{-3}K^{-1}s^{-1}$) which describes the entropy produced due to exchange of matter entering and leaving the SLI with the surrounding [11,34]. The full expressions for both $\dot{\varphi}_{max}$ and $\dot{s}_E$ are respectively given as:

$$\dot{\varphi}_{max} = \frac{\Delta \rho_k \, V^3}{2 \, \zeta^2 \, G_L} \quad (3)$$

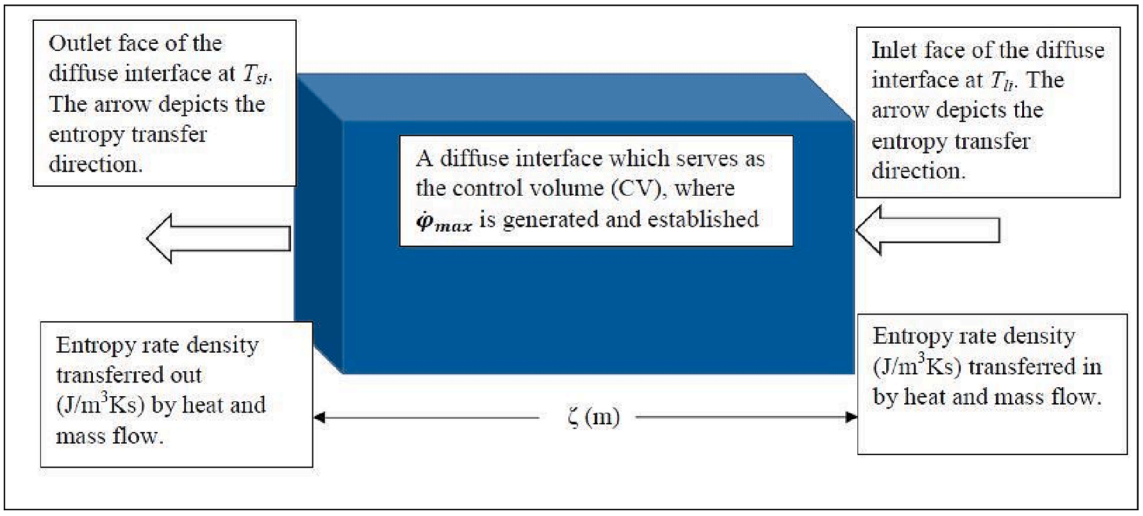

Fig. 1. A schematic illustration of a diffuse interface where entropy is generated and maximized. During solidification, the interface moves with a fixed growth velocity from left to right where the thickness of the interface is, ζ (m) is the control voulme. The diffuse interface region is a mixture of particles from the fully liquid zone and from the fully crystalline zone [16].

$$\dot{s}_E = \frac{V\,\Delta h_m\,G_L\,\rho_s}{T_m^2\,A_w} \tag{4}$$

where $\Delta\rho_k$ (kg m^{-3}) is the overall density shrinkage given by ($\rho_l\,\Delta\rho/\rho_s$), $\Delta\rho$ (kg m^{-3}) is the density change from liquid to solid (ρ_s-ρ_l); ρ_s (kg m^{-3}) and ρ_l (kg m^{-3}) are the densities of the fully solid and fully liquid zones respectively. Also, V (ms^{-1}) is the solidification growth velocity and G_L (Km^{-1}) is the temperature gradient in the liquid zone, T (K) is the melting temperature of the material, Δh_m (Jmol^{-1}) is the heat of fusion, A_w (kgmol^{-1}) is the atomic weight of the material. The SLI (or diffuse interface) is responsible for the microstructural evolution of both faceted and non-faceted morphologies and the corresponding transition from a faceted to non-faceted morphology. The nature of the SLI can be understood by considering the view point of Cahn [10,15] such that, the diffuseness parameter, g_m (*dimensionless*) can be used to predict the nature of the interface during liquid–solid phase transformation, which herein is named as Cahn diffuseness parameter, given by [4,13]:

$$g_m = 2\pi^4\eta_G^3\exp\left(\frac{-\pi^2\eta_G}{2}\right) \tag{5}$$

where the parameter η_G (dimensionless) as introduced by Cahn, describes the size of the interface, ζ (m) on the basis of the number of lattice planes (or the number of atomic layers) [4,13].

This parameter (η_G) is named in this paper as the Cahn driving force diffuseness [17,34] given as:

$$\eta_G = \frac{\zeta}{d} \tag{6}$$

where d (m) is the interplanar spacing of the growth plane preferably along the closed packed plane or otherwise by the plane chosen by the interface, which serves as the appropriate length scale for normalization. Cahn has already shown that the criterion for predicting the formation of a faceted or non-faceted morphology is based on the Cahn diffuseness parameter (g_m) which is dependent on η_G. Although, Cahn was unable to show how η_G could be obtained, recent works has shown that, it can be calculated from experimental data using the maximum entropy production rate density approach [11,12]. Therefore, the Cahn diffuseness concept can be studied on how g_m changes with respect to η_G on the basis of faceted to non-faceted transition. Correspondingly, a criterion for the transition from faceted to non-faceted morphology can be derived based on the Cahn driving force diffuseness (η_G).

Firstly, let us consider the transition from a plane front to a faceted morphology, and thereby taking a derivative of Cahn diffuseness parameter as given in equation (5) with respect to η_G gives:

$$\frac{dg_m}{d\eta_G} = 6\pi^4\eta_G^2\exp\left(-\frac{\pi^2\eta_G}{2}\right) - \pi^6\eta_G^3\exp\left(-\frac{\pi^2\eta_G}{2}\right) \tag{7}$$

For atomistically smooth interface (leading to cellular-faceted morphology), dg_m in equation (7) is expected to change from g_m up to one, and neglecting negative values since they may not have any practical meaning. Also, it is considered that, $d\eta_G$ can change from very small value approaching zero and can grow up to a maximum of one ($0 \rightarrow 1$) for the evolution of cellular faceted morphology. Therefore, integrating equation (7) by the limits explained above gives:

$$\int_{g_m}^{1} dg_m = \left[6\pi^4\int_0^1\eta_G^2\exp\left(\frac{-\pi^2\eta_G}{2}\right)d\eta_G - \pi^6\int_0^1\eta_G^3\exp\left(\frac{-\pi^2\eta_G}{2}\right)d\eta_G\right]$$

$$1 - g_m = 6\pi^4\frac{2!}{(\pi^2/2)^3}\left[1 - \sum_{i=0}^{\eta_G=2}\frac{\left(\frac{\pi^2}{2}\right)^0}{0!} + \frac{\left(\frac{\pi^2}{2}\right)^1}{1!} + \frac{\left(\frac{\pi^2}{2}\right)^2}{2!}\right] - \pi^6\frac{3!}{(\pi^2/2)^4}\left[1 - \sum_{i=0}^{\eta_G=3}\frac{\left(\frac{\pi^2}{2}\right)^0}{0!} + \frac{\left(\frac{\pi^2}{2}\right)^1}{1!} + \frac{\left(\frac{\pi^2}{2}\right)^2}{2!} + \frac{\left(\frac{\pi^2}{2}\right)^3}{3!}\right]$$

$$|g_m| = 0.4 \tag{8}$$

Putting back equation (8) into equation (5) or (considering a plot of g_m against η_G as per equation (5)), which give two solutions to the Cahn driving force diffuseness, that is, η_G is approximately equal to 0.17 (minimum) and 1.5 (maximum), respectively. From the two solutions of η_G, the maximum value is preferred because, the transition from a plane front to a cellular faceted morphology reaches its highest value at when entropy generation at the interface is maximized. And therefore, the Cahn driving force diffuseness inherently becomes:

$$\eta_G = 1.5 \tag{9}$$

Secondly, we consider again for a transition from cellular faceted to cellular non-faceted morphology, where dg_m is expected to grow from 0.4 as in equation (8) to g_m ($0.4 \rightarrow g_m$) while $d\eta_G$ is expected to continue to grow from 1.5 as given in equation (9) to infinity ($1.5 \rightarrow \infty$). Hence, integrating equation (7) by the limit conditions set above, gives:

$$\int_{0.4}^{g_m} dg_m = \left[6\pi^4\int_{1.5}^{\infty}\eta_G^2\exp\left(\frac{-\pi^2\eta_G}{2}\right)d\eta_G - \pi^6\int_{1.5}^{\infty}\eta_G^3\exp\left(\frac{-\pi^2\eta_G}{2}\right)d\eta_G\right]$$

$$g_m - 0.4 = 6\pi^4\left|-\eta_G^2\frac{\exp\left(\frac{-\pi^2\eta_G}{2}\right)}{\left(\frac{\pi^2}{2}\right)} - 2\eta_G\frac{\exp\left(\frac{-\pi^2\eta_G}{2}\right)}{\left(\frac{\pi^2}{2}\right)^2} - 2\frac{\exp\left(\frac{-\pi^2\eta_G}{2}\right)}{\left(\frac{\pi^2}{2}\right)^3}\right|_{1.5}^{\infty} -$$

$$\pi^6\left|-\eta_G^3\frac{\exp\left(\frac{-\pi^2\eta_G}{2}\right)}{\left(\frac{\pi^2}{2}\right)} - 3\eta_G^2\frac{\exp\left(\frac{-\pi^2\eta_G}{2}\right)}{\left(\frac{\pi^2}{2}\right)^2} - 6\eta_G\frac{\exp\left(\frac{-\pi^2\eta_G}{2}\right)}{\left(\frac{\pi^2}{2}\right)^3} - \frac{\exp\left(\frac{-\pi^2\eta_G}{2}\right)}{\left(\frac{\pi^2}{2}\right)^4}\right|_{1.5}^{\infty}$$

$$g_m = 0.0007197 \tag{10}$$

Again, putting back equation (10) into equation (5) or (from a plot of g_m against η_G as per equation (5)), which give two solutions to the Cahn driving force diffuseness, that is, η_G equal to 0.016 (minimum) and 3.3 (maximum), respectively. From the two solutions of η_G, the maximum is preferred because, highest value is reached when entropy generation at the interface is maximized. And therefore, this sets the criterion for the transition from a cellular faceted morphology to a cellular non-faceted morphology as:

$$\eta_G = 3.3 \tag{11}$$

Note that from the criterion set in equation (11), the faceted cells (at $\eta_G = 1.5$) must grow to a matured cellular morphology before transformation to a non-faceted morphology is achieved.

Analysis of transition criterion in the context of MEPR

The solid–liquid interface (SLI), which is responsible for the morphological variants in an open thermodynamic system allows the exchange of both matter and energy between the fully solid and fully liquid zones in a unidirectional way. The flow of atoms to the control volume and the movement of atoms/crystallites to the fully solid zone, and the continuous movement of the interface generates an irreversible entropy which reaches a maximum when a new morphology emerges [11,12,17,53-58 16,59-67 68]. This maximization of the entropy generated has been analysed by many under the maximum entropy generation/production rate (MEPR) principle. Sekhar [16,59] defines it that, if there are sufficient degrees of freedom within a system, it will adopt a stable state at which the entropy generation/production rate would be maximized.

The theoretical bases of MEPR, formulated independently by Ziman [68] and Ziegler [69] reveals pathway selection rules for any given system [16,56,57,70-72]. While MEPR has seen wide applications across many disciplines, Kirkaldy [73], Martyushev, Seleznev and Kuznetsova [65], and Sekhar [16] have also shown that, for a unidirectional crystal growth from the melt, the SLI morphological instability can be analyzed with the MEPR principle. Previous studies on the application of MEPR principle to solidification/crystal growth processes (MEPR model) showed that the entropy generation is maximized for an interface transition to a different morphological variant and that, the highest entropy rate producing configuration is the most stable [11,12,17]. In his seminal paper, Sekhar [16] derived series of fundamental and foundational equations based on MEPR to track SLI instability and thickness. Later, Bensah [11,12] extended the MEPR model and showed that the maximum entropy generation rate density is achieved when the moving interface losses work due to entropy generation through heat dissipation [11,34 11,12]. Also, the derived quantitative expression for the maximum entropy production rate density, $\dot{\varphi}_{max}$ ($Jm^{-3}K^{-1}s^{-1}$) associated with the SLI during solidification is given as in equation (3) [11,12,17]. And as such, the criterion for transition from cellular faceted to non-faceted cellular morphology is expected to obey equation (3).

From equation (3), the value of $\dot{\varphi}_{max}$ reaches a minimum when equilibrium is established, noting that the diffuse interface is created only when the solidification velocity is greater than the minimum. For all forms of non-associated morphological change, an increase in $\dot{\varphi}_{max}$ corresponds to a decrease in the size of the interface. However, for any form of morphological change (morphological instability and beyond) there is an extra burst/surge of entropy generated that stretches the interface in proportion to the change in solidification growth velocity. Equations (2), (3) and (4) can be combined to evaluate the size of the interface for a faceted to non-faceted transition given as:

$$\zeta = \frac{V}{G_L}\sqrt{\frac{\Delta\rho_k\, T^2_{m\,A_w}}{2\,\Delta h_m\,\rho_s}} \tag{12a}$$

Equation (12a) can be written in a more condensed and compact form when combine with equation (6) to give:

$$\eta_G = M_d\sqrt{\frac{\Delta\rho}{\rho_s}} \tag{12b}$$

where the symbol M_d (dimensionless) represents the expression $\left(V\,T_M\sqrt{A_w}\,/G_L\,d\sqrt{2\Delta h_m}\right)$. The role of the component $\sqrt{A_w}T_M\,/d\sqrt{2\Delta h_m}$ (Ksm^{-2}) in M_d is to modify the dimension of the V/G_L ($m^2s^{-1}K^{-1}$) ratio and to enable normalization of M_d into a dimensionless form. The value of M_d is highly dependent on the V/G_L ratio ($m^2K^{-1}s^{-1}$), especially V, which is the main variable in any typical directional solidification process. An expected linear relationship is observed when η_G is plotted against M_d, and where at $\eta_G = 3.3$ will correspond to faceted to non-faceted transition. So, for a faceted to non-faceted transition, equation (12b) is combined with equation (11) to give:

$$M_d = 3.3\sqrt{\frac{\rho_s}{\Delta\rho}} \tag{13a}$$

The importance of equation (13a) is that, the transition value of M_d can be evaluated without the knowledge of the V/G_L ratio ($m^2K^{-1}s^{-1}$). Further, reorganization of equation (13a) gives the solidification growth velocity required for a cellular faceted to non-faceted transition to occur as:

$$V_{f-nf} = \frac{14\,G_L\,d\,\sqrt{\rho_s\,\Delta h_m}}{3\,T_M\,\sqrt{\Delta\rho\,A_w}} \tag{13b}$$

The transition growth velocity in equation (13b) can be written in a dimensionless form as:

$$\overline{V}_{f-nf} = \frac{14\,G_L\,d}{3\,T_M}\sqrt{\frac{\rho_s}{\Delta\rho}} \tag{13c}$$

where $\overline{V}_{f-nf}$ is a dimensionless transition growth velocity expressed as $\left(V_{f-nf}\sqrt{A_w}\,/\sqrt{\Delta h_m}\right)$. The evolution of the cellular faceted morphology is accompanied by an associated size. At any given solidification velocity beyond instability, the size of the cellular morphology, λ (m), either faceted or non-faceted, has been derived as [12];

$$\lambda^3 = \frac{2\,\pi\,\gamma_{gb}\,a_o\,\zeta}{\Delta\rho_k\,V^2} \tag{14}$$

where a_o (m) is the lattice parameter and γ_{gb} (Jm^{-2}) is the grain boundary energy. Combining equations (11), (13b) and (14) gives the cellular size at the morphological transition from cellular faceted to cellular non-faceted as;

$$\lambda_{f-nf} = \sqrt[6]{h^{2+}k^2 + l^2}\,\sqrt[3]{\frac{A_w\,\gamma_{gb}\,T_m^2}{G_L^2\,\rho_s\,\Delta h_m}} \tag{15}$$

where the *h*, *k*, *l* values are the Miller indices that gives the growth plane of the transition as chosen by the interface.

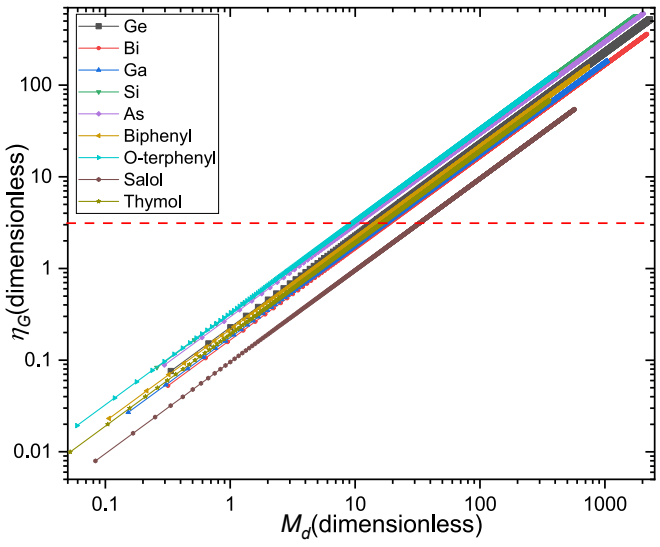

Fig. 2. Model prediction for the driving force diffuseness η_G (dimensionless) as against M_d (dimensionless) for pure materials showing both atomically smooth and rough interfaces as according to equation (12b). The driving force diffuseness is calculated from a fixed temperature gradient and a varied growth velocity. The dotted red horizontal line indicates the transition from facet to non-facet morphological forms. (For interpretation of the references to colour in this figure legend, the reader is referred to the web version of this article.)

Table 2
Some physical properties for the pure materials.

Material	Atomic weight ($Kgmol^{-1}$) [74]	Melting Temp T_M (K)	ρ_s of solid at T_R (Kgm^{-3}) [75]	ρ_l of liquid at T_M (Kgm^{-3}) [75]	Heat of fusion Δhm ($Jmol^{-1}$)	Heat of fusion Δh_{sl} (Jm^{-3}) × 10^8	d (nm)	Crystal structure
Germanium	0.0726	1211.4	5323	5600	36,940	27.073	0.327	Diamond cubic
Bismuth	0.2089	544.7	9780	10,050	11,300	5.288	0.475	Rhombohedral
Gallium	0.0697	302.915	5910	6095	5590	4.738	0.451	Orthorhombic
Silicon	0.0281	1687	2329	2570	50,210	41.638	0.314	Diamond cubic
Grey Arsenic	0.0749	1090	5727	5220	24,440	18.682	0.413	Trigonal
Biphenyl	0.1542	343.15	1040	991.4	19,900	1.28	0.573	Hexagonal
O-terphenyl	0.2304	330.15	1160	1036	17,190	0.773	1.314	Hexagonal
Salol	0.2143	315.65 [76]	1191.1 at 303.65 K [76]	1180.2 [76]	19,160 [77]	1.06	0.814	Orthorhombic
Thymol	0.1502	324.2	960	925	22,010	1.36	0.104	Hexagonal

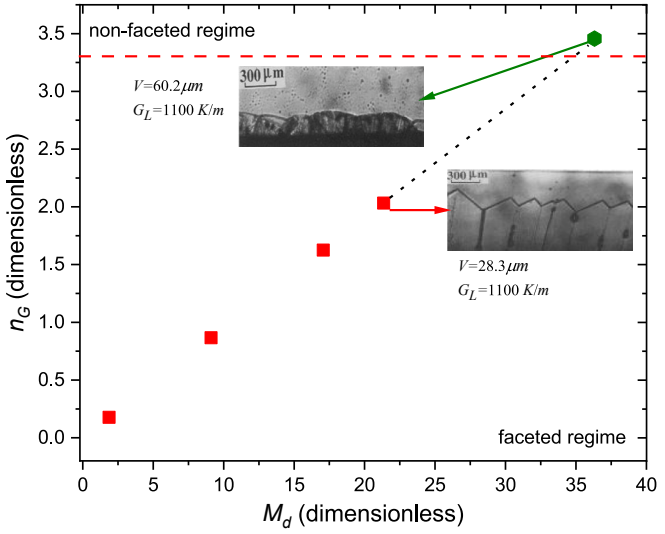

Fig. 3. A plot of calculated η_G (dimensionless) against M_d (dimensionless), which gives a linear relationship according to equation (12) for salol. The parameter M_d strongly depends on the V/G_L ($m^2K^{-1}s^{-1}$) ratio. The V/G_L ($m^2K^{-1}s^{-1}$) ratios are from published experimentally measured data as given in table-3. The value of $\sqrt{\rho_s/\Delta\rho}$ is the slope (0.10 Ks/m) of the line. The plot shows the transition from faceted morphology to non-faceted morphology with increasing velocity as shown for dotted black diagonal line. The inserted images [32] are from experimental data and show the interface morphologies formed during the transition. The horizontal dotted red line represents the transition boundary between faceted morphology to non-faceted morphology. (For interpretation of the references to colour in this figure legend, the reader is referred to the web version of this article.)

Results and discussions

The application of Cahn's theory of interface diffuseness has been used to arrive at a transition criterion for faceted to non-faceted cellular morphology. The application was based on the maximum entropy production rate (MEPR) principle, used as a selection rule for morphological pattern formation for the case of steady state directional solidification. The MEPR approach is shown to have a decisive influence on morphological pattern formation and the critical parameters that govern their selection when considering morphological transition and stability [11,12,17]. The model predictions for pure faceting materials that are able to transition into non-faceting form are given in Fig. 2 and corresponding data given in Table 2. The model derivations in equations (11–13) have shown that, the faceted to non-faceted cellular transition occurs when the interface grows from 3.3 atomic layers as given by the horizontal dotted line shown in Fig. 3. That is, horizontal dotted line serves as a transition boundary between faceted and non-faceted cellular morphology. In Fig. 3, the plot of η_G against M_d which is based on experimentally measured values of V/G_L, shows that the points formed around and close to the horizontal dotted-red-line (border line) have the potential to form faceted or non-faceted morphologies depending on the growth velocity, temperature gradient and crystallographic plane chosen by the interface as per equation (12). The corresponding data for Fig. 3 is given in Table 3. Although there are only a few experimental studies on the factors that influence *f-nf* transitions, however, it has been noted that both the temperature gradient and transformation growth velocity play a major role for such a transformation as captured in equation (12).

Again, Fig. 3 provides a visual explanation of how salol can transition from faceted morphology to non-faceted morphology with increasing velocity, which is an example of the effect of driving force diffuseness as predicted theoretically by Cahn [10,15] and the current MEPR model as shown in equation (12). Note that, such transitions in many materials have been recorded [32,37-45] as given in Table 1. The Cahn model [4,13] which showed for the first time that diffuseness was a function of the growth velocity was unable to make clear quantitative predictions for the onset of faceted to non-faceted morphology. Other experimental observations confirm that, pure bismuth, salol, germanium, benzyl, silicon, water etc., have the ability to exhibit both faceted and non-faceted morphologies at different crystallographic orientations and undercooling (or temperature gradients) [30,31]. These experimental observations are in agreement with the predictions made by equation (13). Also, equation (13) shows that the *f-nf* transition is dependent on the temperature gradient and solidification growth velocity. The cellular size at the transition can be evaluated from equation (15) and as demonstrated for salol in Table 3. For salol at a temperature gradient of 1100 km^{-1}, the transition cellular size is 309 μm. In addition, Fig. 4 is added to give microstructural assessment of the first transition from a plane front to a cellular faceted morphology for salol. This is supported by the tabulated results in Table 4 where the cellular size calculations for salol at instability are given for different temperature gradients and using a fixed solidification velocity from experimental data. The calculated cellular size results show closeness when comparison is made with experimental results, and shows that they are in the same order of magnitude. The results are much more appreciable at lower temperature gradients, where the deviations from experimental values are within an

Table 3
Experimental data and results of calculated parameters for salol, where the growth was considered for the (100) plane.

Material	Experimental data		Results of calculated parameters from model using equations (13b) and (15) respectively				
	V (μms^{-1})	G_L (Km^{-1})	ζ	η_G	M_d	$V_{f\text{-}nf}$ (μms^{-1})	$\lambda_{f\text{-}nf}$ (μm)
Salol[1]	28.3	1100	1.83	1.625	17.067	57.2	309
Salol[2]	60.2		3.89	3.457	36.306		
Salol[3]	15.1		0.98	0.867	9.107		
Salol[4]	3.10		0.20	0.178	1.869		
Salol[5]	35.4		2.29	2.033	21.349		

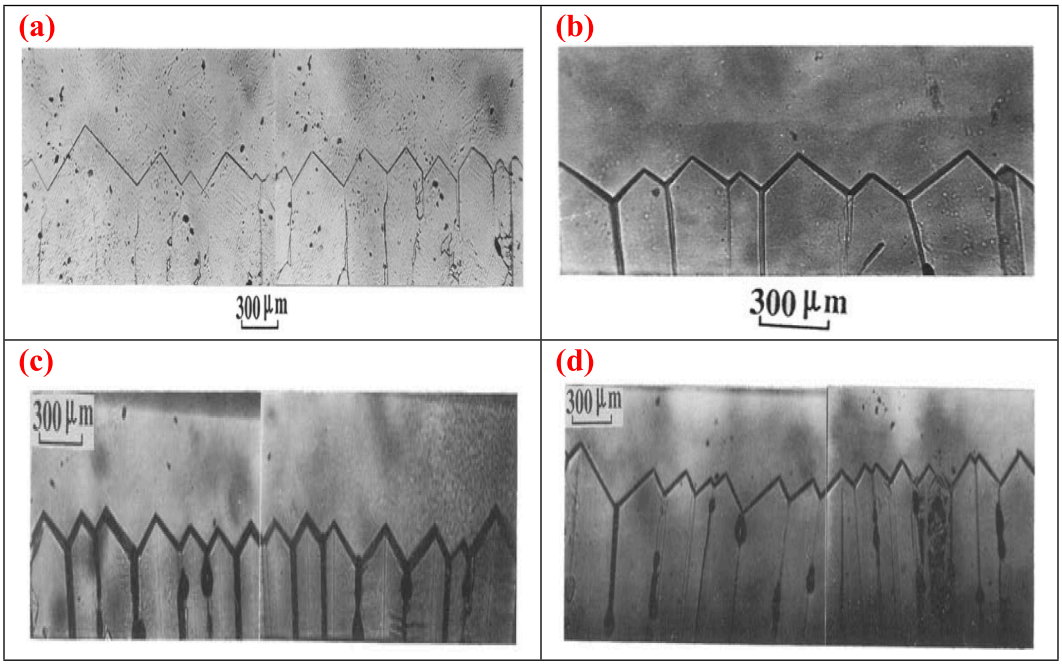

Fig. 4. This shows typical micrographs of faceted morphology for salol as a result of a plane front transition as measured by Shangguan [32]. The micrographs are for (a) V = 8.6 μms^{-1} at 52 Kcm^{-1} (b) V = 28.3 μms^{-1} at 18 Kcm^{-1} (c) V = 8.6 μms^{-1} at 18 Kcm^{-1} (d) V = 28.3 μms^{-1} at 11 Kcm^{-1}.

Table 4
Calculated results of cellular size at interface instability (from plane front to faceted morphology) compared with experimental data results for salol at a fixed velocity of 3.3 μms^{-1}[12]. This corresponds to a transition value of η_G equal to 1.5 as per equation (9). The experimental data used were obtained from Shangguan [32].

Temperature gradient G_L (Km^{-1})	Cellular size λ_C (μm)		Calculated cell size deviation from experiment
	Experiment	MEPR	$\lvert 1-\lambda_{expt}/\lambda_{MEPR}\rvert$
6500	520	234	1.22
3500	560	354	0.58
1800	640	551	0.16
1100	670	765	0.12

Table 5
Calculated results of cellular size beyond interface instability (matured cells) compared with experimental data salol [12]. The calculated results are from equation (14). The experimental data used were obtained from Shangguan [32].

Data obtained from experiment			Calculated parameters from current work using experimentally measured velocity		Calculated cell size deviation from experiment
G_L (Km^{-1})	V (μm/s)	λ_{exp} (m)	ζ (nm)	λ_{MEPR} (μm)	$\lvert 1-\lambda_{expt}/\lambda_{MEPR}\rvert$
6500	3.30	520	0.076	346	0.504
3500	5.70	560	0.132	288	0.700
1800	3.30	640	0.142	425	0.317
1100	15.1	670	0.649	256	0.102

appreciable limit [12,32]. From the data in Table 5, equation (14) is tested for salol with experimental data at solidification growth velocities beyond the transition instability condition, i.e., for fully grown or matured cellular patterns. The predictions for the calculated cellular size for salol is given at different temperature gradient and solidification velocities. The calculated results show reliability of the model as it shows closeness to experimental measurements [12,32].

Conclusion

By the analysis of the Cahn's diffuseness equation, we are able to arrive at transition criterion for cellular faceted to non-faceted morphology during liquid–solid transformation. This happens when the driving force diffuseness is at 3.3. The criterion is combined with the MEPR expression for the driving force diffuseness to arrive at the transition growth velocity and maximum entropy production rate density for a faceted to non-faceted transition and the size of the cellular morphology at transition.

Ethics statement

This work does not involve any activity of human or biological materials or content.

Data accessibility

The experimental data used were from already published data and are appropriately referenced in the article.

Competing interests

The author is not aware of any competing interests to the best of his knowledge.

Authors' contributions

The entire work was conceived and completed solely by the author.

Funding statement

This work was supported through the author's personal funds.

Declaration of Competing Interest

The author declares that there is no known competing financial interests or personal relationships that could have appeared to influence the work reported in this paper.

Data availability

All data used are tabulated in the paper.

Acknowledgement

Appreciation to Ms. Gwendolyn Naa Oyo Quartey for reading through the manuscript.

References

[1] Kang H, Wanga T, Li X, Su Y, Guo J, Fu H. Faceted–nonfaceted growth transition and 3-D morphological evolution of primary Al_6Mn microcrystals in directionally solidified. J Mater Res 2014;29(11):1256–63.
[2] Hyde KB, Norman AF, Prangnell PB. The effect of cooling rate on the morphology of primary Al_3Sc intermetallic particles in Al–Sc alloys. Acta Mater 2001;49:1327–37.
[3] Fisher DJ, Kurz W. A theory of branching limited growth of irregular eutectics. Acta Metall 1980;28:777–94.
[4] Sato T, Sayama Y. Eutectic growth of unidirectionally solidified iron-carbon alloy. J Cryst Growth 1974;22(2):272–86.
[5] Xian JW, Belyakov SA, Ollivier M, Nogita K, Yasuda H, Gourlay CM. Cu6Sn5 crystal growth mechanisms during solidification of electronic interconnections. Acta Mater 2017;126:540–51.
[6] Qin Q, Li W. The Formation and Characterization of the Primary Mg2Si Dendritic Phase. Mater Trans 2016;57(2):85–90.
[7] Qin QD, Zhao YG, Zhou W, Cong PJ. Effect of phosphorus on microstructure and growth manner of primary Mg2Si crystal in Mg2Si/Al composite. Mater Sci Eng A 2007;447:186–91.
[8] Qin QD, Zhao YG, Liu C, Cong PJ, Zhou W. Strontium modification and formation of cubic primary Mg2Si crystals in Mg2Si/Al composite. J Alloy Compd 2008;454:142–6.
[9] Flemings MC. Solidification Processing. McGraw: McGraw Hill; 1974.
[10] Cahn J. Theory of crystal growth and interface motion in crystalline materials. Acta Metall 1960;8:554.
[11] Bensah YD. Morphological linstability at the solid-liquid interface by the maximum entropy production rate principle. Can J Phy 2018;96(12).
[12] Bensah YD. Evolution of cellular morphology in pure materials. J Mater Sci 2020:1–16.
[13] Chalmers B. Principles of solidification. New York: John Wiley and Sons; 1964.
[14] Kurz W, Fisher TJ. Solidification. Switzerland: Trans Tech Publications; 2003.
[15] Cahn JW, Hillig WB, Sears GW. The molecular mechanism of solidification. Acta Metall 1964;12:1421–39.
[16] Sekhar JA. The description of morphologically stable regimes for steady state solidification based on the maximum entropy production rate postulate. J Mater Sci 2011;46:6172–90.
[17] Bensah YD, Sekhar JA. Solidification morphology and bifurcation predictions with the maximum entropy production rate model. Entropy 2020;22(40):2–13.
[18] Young T. An essay on the cohesion of fluids. Phil. Trans. R.y Soc. 1805;95:65–87.
[19] P. S. Laplace, "Traite de ḿecanique ćeleste; supplements au Livre X,," in *Euvres, Vol. 4*, Paris, Gauthier-Villars, 1805 and 1806: English translation by N. Bowditch (1839); reprinted by Chelsea, New York, 1966..
[20] C. F. Gauss, "Principia Generalia Theoriae Figurae Fluidorum," *Comment Soc. Regiae Scient. Gottingensis,* vol. 7, 1830.
[21] Lamorgese AG, Molin D, Mauri R. Phase field approach to multiphase flow modeling. Milan J Math 2011;79:597–642.
[22] Wilson HA. Philos Mag 1900;50:238.
[23] Frenkel J. Phys Z Sowjetunion 1932;1:498.
[24] Becker R, Doring W. Ann Phys (Leipzig) 1935;24:719.
[25] Burton WK, Cabrera NT, Frank FC. The growth of crystals and the equilibrium structure of their surfaces. Phil Trans A 1950;243:299.
[26] Rayleigh L. "On the theory of surface forces. II. Compressible fluids. Phil Mag 1892;33:209–20.
[27] J. D. Van der Waals, "The thermodynamic theory of capillarity under the hypothesis of a continuous variation of density," *Verhandel. Konink. Akad. Weten,* vol. 1, no. 8, p. 56, 1893. Translated by "J. S. Rowlinson,J. Stat Phys. Vol. 20, No. 2, 1979, 197-244".
[28] Landau L. "On the theory of phase transitions", Zh. Eksp. Teor. Fiz., vol. 7, pp. 19–32, 1937 Translated by Ukrainian Physico-Technical Institute. Ukr J Phys 2008;(53):25–35.
[29] Jackson KA. Liquid metals and solidification. Cleveland: American Society for Metals; 1958.
[30] Woodruff DP. The solid-liquid interface. London: Cambridge University Press; 1973.
[31] Doremus RH. Rates of phase transformation, Orlando. Florida: Academic Press; 1985.
[32] D. Shangguan, "PhD Thesis," University of Oxford, Oxford, 1989.
[33] Jackson KA. Transparent compounds that freeze like metals. Acta Metall 1965;13:1212–5.
[34] Bensah YD. Interfacial solid-liquid diffuseness and instability by the maximum entropy production rate postulate. Cincinnati: University of Cincinnati; 2015. PhD thesis.
[35] K. A. Jackson, "Growth and Perfection of Crystals," in *Eds. R. H. Doremus, B. W. Roberts and D. Turnbull* , New York, Wiley, 1958.
[36] Jackson KA, Uhlman DR, Hunt JD. On the crystal growth of melt. J Cryst Growth 1967;1:1–36.
[37] Sekhar JA, Bharti A, Trivedi R. Faceted-nonfaceted dendritic transitions during the laser Processing of Al203-1.0 Wt Pct MgO. Metall Trans A 1989;20A:2191–4.
[38] Green JR, Griffith WT. Phase transformation in solid cyclohexanol: Growth rates and morphology from visual observations. J Cryst Growth 1969;5:171–83.
[39] Miller CE. Faceting transition in melt-grown crystals. J Cryst Growth 1977;42:357–63.
[40] Glicksman ME, Schaeffer RJ. Investigation of solid-liquid interface temperatures through isenthalpic solidification. J Cryst Growth 1967;1:297–310.
[41] Rao KN, Sekhar JA. Solidification of the quasi-crystalline phase in the Al-Cu-Li system. Scripta Metall 1987;21:805–10.
[42] Brice JC, Whiffin PAC. The temperature distribution in pulled germanium crystals during growth. Solid State Electron 1964;7:183–7.
[43] Jackson KA, Miller CE. Experimental observation of the surface roughening transition in vapour phase growth. J Cryst Growth 1977;40:169–72.
[44] Passerone A, Eustathopoulos N. Experiemntal study of the solid-liquid equilibrium roughnening transition in Zn-In alloys. J Cryst Growth 1980;49:757–60.
[45] Passerone A, Sangiorgi R, Eustathopoulo N. Isothermal faceted to nonfacted equilibrium transition of solid-liquid interfaces in Zn-Bi-In alloys. Scripta Metall 1980;14:1089–92.
[46] Collins JB, Levine H. Phys Rev B 1985;31:6119.
[47] Langer JS. In: Directions in Condensed Matter. Singapore: World Scientific; 1986. p. 164.
[48] Caginalp G, Fife P. Phys Rev B 1986;B33:7792.
[49] Wheeler AA, Boettinger WJ, McFadden GB. Phys Rev A 1992;45:7424.
[50] Caginalp G, Xie W. Phys Rev E 1993;48:1897.
[51] Warren JA, Boettinger WJ. Acta Metall Mater 1995;A43:689–703.
[52] Plapp M, Karma A. Phys Rev Lett 2000;84:1740.
[53] Gershman I, Mironov A, Podrabinnik P, Kuznetsova E, Gershman E, Peretyagin P. Relationship of secondary structures and wear resistance of antifriction aluminum alloys for journal bearings from the point of view of self-organization during friction. Entropy 2019;21:1048.
[54] Sekhar JA. Tunable coefficient of friction with surface texturing in materials engineering and biological systems. Curr Opin Chem Eng 2018;19:94–106.
[55] Wang W, Zhang Y, Liu J, Wu Z, Li B, Sundén B. Entropy generation analysis of fully developed turbulent heat transfer flow in inward helically corrugated tubes. Numer Heat Transf A-Appl 2018;73:788–805.
[56] Martyushev LM, Seleznev VD. Maximum entropy production: Application to crystal growth and chemical kinetics. Curr Opin Chem Eng 2015;7:23–31.
[57] Veveakis E, Regenauer-Lieb K. Review of extremum postulates. Curr Opin Chem Eng 2015;7:40–6.
[58] Bensah YD, Sekhar JA. Morphological assessment with the maximum entropy production rate postulate. Curr Opin Chem Eng 2014;3:91–8.
[59] Bensah YD, Li HP, Sekhar JA. The Sgen rate maximization postulate: Applications to process-path analysis for solidification and micropyretic synthesis. Key Eng Mater 2012;521:79–86.
[60] Wang H, Liu F, Zhai H, Wang K. Application of the maximal entropy production principle to rapid solidification: A sharp interface model. Acta Mater 2012;60:1444–54.
[61] Chung B, Vaidya A. Non-equilibrium pattern selection in particle sedimentation. Appl Math Comput 2011;218:3451–65.
[62] Sekhar JA, Li HP, Dey GK. Decay-dissipative Belousov-Zhabotinsky nanobands and nanoparticles in NiAl. Acta Mater 2010;58(3):1056–73.
[63] Nosonovsky M. Self-organization at the frictional interface for green tribology. Philos Trans R Soc A 2010;368:4755–74.
[64] Nosonovsky M, Bhushan B. Thermodynamics of surface degradation, self-organization and self-healing for biomimetic surfaces. Philos Trans R Soc A 2009;367:1607–27.
[65] Martyushev LM, Seleznev VD, Kuznetsova IE. Application of the Principle of Maximum Entropy production to the analysis of the morphological stability of a growing crystal. Zh Éksp Teor Fiz 2000;118:149.
[66] Hill A. Entropy production as the selection rule between different growth morphologies. Nature 1990;348:426–8.
[67] Ziegler H, Wehrli C. On a principle of maximal rate of entropy production. J Non-Equilib Therm 1978;12:229.
[68] Ziman JM. The general variational principle of transport theory. Can J Phys 1956;35:1256.
[69] H. Ziegler, An introduction to thermomechanics, Amsterdam: North- Holland, 1983.
[70] Swenson R. Spontaneous Order, Autocatakinetic closure, and the development of space-time. Ann NewYork Acad Sci 2000;901:311–9.
[71] Sekhar JA. The shape of materials engineering for the next 100 years. Curr Opin Chem Eng 2015;7:1–4.
[72] Wang H, Zhang X, Lai C, Kuang W, Liu F. Thermodynamic principles for phase-field modeling of alloy solidification. Curr Opin Chem Eng 2015;7:6–15.

[73] Kirkaldy JS. Entropy criteria applied to pattern selection in systems with free boundaries. Metall Trans A 1985;16A:1781–96.
[74] Chemistry IUPAC. Atomic weight of elements. Handbook 1981;55(7):1101–36.
[75] W. F. Gal and T. C. Totemeier(editors), "Smithells metals reference book," *Elsevier Inc.,* vol. 8th edition, 2004.
[76] Badachhape RB, Gharpurey MK, Biswas AB. Density and surface tension of phenol, (mono-, di-, and tri-) chlorophenols, salol, and (0- and rn-)chloronitrobenzenes. J Chem Engrg Data 1965;10(2):143–5.
[77] Hanaya M, Hikima T, Hatase M, Oguni M. Low-temperature adiabatic calorimetry of salol and benzophenone and microscopic observation of their crystallization: finding of homogeneous-nucleation-based crystallization. J Chem Thermodyn 2002;34(8):1173–93.